







Advances in Space Research

Volume 53, Issue 12, 15 June 2014, Pages 1735-1767

Construction of lunar DEMs based on reflectance modelling

Arne Grumpe  , Fethi Belkhir , Christian Wöhler 

Show more 



Share



Cite

<https://doi.org/10.1016/j.asr.2013.09.036> 

[Get rights and content](#) 

Abstract

Existing lunar DEMs obtained based on laser altimetry or photogrammetric image analysis are characterised by high large-scale accuracies while their lateral resolution is strongly limited by noise or interpolation artifacts. In contrast, image-based photometric surface reconstruction approaches reveal small-scale surface detail but become inaccurate on large spatial scales. The framework proposed in this study therefore combines photometric image information of high lateral resolution and DEM data of comparably low lateral resolution in order to obtain DEMs of high lateral resolution which are also accurate on large spatial scales. Our first approach combines an extended photoclinometry scheme and a shape from shading based method. A novel variational surface reconstruction method further increases the lateral resolution of the DEM such that it reaches that of the underlying images. We employ the Hapke IMSA and AMSA reflectance models with two different formulations of the single-particle scattering function, such that the single-scattering albedo of the surface particles and optionally the asymmetry parameter of the single-particle scattering function can be estimated pixel-wise. As our DEM construction methods require co-registered images, an illumination-independent image registration scheme is developed. An evaluation of our framework based on synthetic image data yields an average elevation accuracy of the

constructed DEMs of better than 20m as long as the correct reflectance model is assumed. When comparing our DEMs to LOLA single track data, absolute elevation accuracies around 30m are obtained for test regions that cover an elevation range of several thousands of metres. The proposed illumination-independent image registration method yields subpixel accuracy even in the presence of 3D perspective distortions. The pixel-wise reflectance parameters estimated simultaneously with the DEM reflect compositional contrasts between different surface units. Specifically, the detected variations of the parameter of the single-particle scattering function indicate small-scale variations of the regolith particle size, possibly as a result of differences in soil maturity.

Introduction

The reconstruction of 3D surfaces based on 2D images has been of scientific interest for decades. However, most of the work is based solely on images while little work has been done on the fusion of photometric information, e.g. images, and absolute depth data, e.g. active range scanning, which has become available for a broad range of applications. We present an approach to reconstruct a 3D surface model, a so-called digital elevation model (DEM), from photometric measurements combined with absolute depth data of lower lateral resolution and synchronous estimation of the reflectance model. The result is a DEM which has the same lateral resolution as the image and the a vertical accuracy comparable to that of the absolute depth data. The algorithm is applied to regions of the lunar surface. This section motivates the proposed approach especially in the field of planetary DEM construction, presents a brief overview over related works throughout the literature, and introduces the dataset.

Since planetary bodies tend to be large, remotely obtained data are important for the global understanding of a planet. Field sampling, e.g. core samples and laboratory measurements, are not feasible due to the large size of the investigated bodies. Thus, spatially comprehensive samples may only be acquired remotely. Furthermore, extraterrestrial planetary bodies simply are too far away for field samples. Within remote sensing, imagery is of high interest as it allows remote sampling of large areas at high lateral resolution. Applications range from high-resolution photographs, which are used for photogeologic interpretation of the surface structure, to hyperspectral imagery where images are taken across broad wavelength intervals. The latter technique is used to derive the reflectance behaviour of the surface at a large number of distinct wavelengths and infer the mineral composition of the surface (Mustard and Pieters, 1989).

However, the measured spectral radiance and thus the spectral reflectance highly depend on the surface topography. This is illustrated in Fig. 1 which shows the spectral reflectance of the same surface area when the surface is illuminated by the sun from the east (blue) and from the west (black). The area of interest is located on the eastern side of a crater rim and thus shaded and brightened, respectively. To avoid misinterpretations of this distortion, the reflectance has to be normalised with respect to local topography.

Such a normalisation procedure requires a DEM which is co-registered with the image and has at least the same lateral resolution. Since the reflectance depends on the surface inclination, a DEM of two or three times the lateral image resolution would be preferable. However, in the case of the Moon no available DEM, including the gridded Lunar Orbiter Laser Altimeter (LOLA) DEM and the GLD100 which are introduced in detail in Section 1.4, globally matches the lateral resolution of modern hyperspectral data. In order to increase the lateral resolution of existing DEMs, we developed an approach to fuse the photometric information of the hyperspectral imagery with the absolute depth data of the available DEMs. The resulting refined DEM has the same lateral resolution as the images.

Besides the surface slope, the spectral reflectance depends on local surface properties, such as grain size and albedo, which may be wavelength dependent and therefore lead to a wavelength dependence of the parameters of the reflectance function. Hence, the resulting spectral reflectance may exhibit distortions (cf. Fig. 1(c)), such that the integrated estimation of surface topography and surface properties becomes inevitable. The spectral reflectance is thus normalised with respect to the surface topography and the local parameters of the reflectance function. Although the reconstruction of the surface topography can be based on a single channel of a multispectral or hyperspectral image sensor, the reflectance parameter estimation has to be applied to each channel separately, resulting in a pixel-wise spectrum of reflectance parameters.

In this paper, the terms “photoclinometry” (PHCL) and “shape from shading” (SfS) are used frequently. Both terms are often considered as synonyms, denoting the recovery of topography from intensity or shading information, e.g. reflectance, in images. Historically, the term photoclinometry originates from planetary science while shape from shading was developed in the machine vision community. There are, however, a couple of differences within both methods. Here, we follow the reasoning of Horn (1990). However, it is no longer possible to distinguish between profile and area-based techniques due to the more recent development of area-based inclination estimation approaches. The main difference that we use to distinguish between both methods are as follows:

- The term photoclinometry originates from the photometric estimation of inclinations, i.e. surface slopes (van Diggelen, 1951, Davis et al., 1984). A subsequent, often neglected step is the integration of the estimated surface slopes which yields an estimate of the surface.
- Shape from shading aims at an integrated approach to determine surface inclination and height.

The area-based reconstruction schemes solve directly for the elevations but are still labelled “photoclinometry” by most planetary scientists. Nevertheless, our complementary algorithms can be divided into one algorithm that directly estimates the elevations while the other one estimates the surface slopes and computes the DEM in a subsequent step. Therefore, we regard it as useful to distinguish between both methods by referring to the determination of gradients as photoclinometry and the direct determination of elevations as shape from shading.

In contrast to common photogrammetric surface construction techniques, e.g. bundle adjustment and stereo image processing (McGlone et al., 2004), which generally yield DEMs at lateral resolutions one order of magnitude lower than the image resolution (Kirk et al., 2003a, Schenk, 2008, Scholten et al., 2012), photometric or intensity-based methods regard the imaging device as a sensor measuring brightness that gives clues about the surface inclination. Hence, photometric methods estimate a surface which is co-registered with the original image. Furthermore, photometric methods, e.g. shape from shading, are able to construct DEMs based on single images.

The remainder of this section is structured as follows. First, the state of the art of photometric surface estimation methods is presented. Finally, we will review reflectance models that are common in planetary science. These models are a necessity for any topography reconstruction method.

Early work on the estimation of slopes and heights from photometric data was based on image profiles (van Diggelen, 1951, Davis et al., 1984). Pioneering methods for area-based 3D surface reconstruction based on image intensity information were introduced by Horn, 1970, Horn, 1975. Similar approaches to the estimation of topographic data from photometric image information, sometimes referred to as 2D-photoclinometry, were developed by Wildey, 1975, Kirk, 1987.

Horn (1990) provides an extensive survey of the development of photometric methods. Most of them focus on the estimation of gradients from shading information since the proportion of light reflected from a surface depends on the surface slope rather than the

absolute height. Furthermore, Horn (1990) presents a coupled scheme for simultaneous estimation of surface height and gradients. This method will be referred to as “shape from shading”. Since our work is based on the SfS method by Horn (1990), this method will be reviewed in detail in Section 3.3.

Since most photometric methods estimate the surface gradient field, the integrability of estimated surface gradients and the estimation of the surface height has been of large interest to the community. Solutions are presented by Frankot and Chellappa, 1988, Horn, 1990, Agrawal et al., 2006. The approach by Horn (1990) is based on a variational optimisation by minimising the quadratic Euclidean distance between gradient field of the estimated surface and the measured gradient fields. This method leads to a Poisson equation and is described in detail in Section 3.2. The method by Frankot and Chellappa (1988) is based on the projection of the gradient field onto the set of integrable Fourier basis functions. However, the employed discrete Fourier transformation requires uniform ground pixel sizes, which is not valid for the cylindrical projection we use as data representation. Agrawal et al. (2006) gives an extensive overview of existing surface gradient integration schemes and presents a formal description leading a continuum of solutions including the solutions by Horn, 1990, Frankot and Chellappa, 1988.

While an extensive body of literature exists on shape from shading and shape recovery from photometric measurements, the fusion of photometric information and absolute depth measurements, such as laser range scanning or geometrical methods like stereo analysis or bundle adjustment, has been developed within the last decade. Soderblom et al. (2002) propose a method to identify the parameters of the reflectance model such that the height profile obtained from Mars Orbiter Narrow Angle Camera images matches a track of laser range scanning single point measurements of the Mars Orbiter Laser Altimeter in a least squares sense. The resolution of the resulting profile is one to two orders of magnitude larger than the resolution of the laser profile. An extension towards an area-based method that uses gridded and interpolated Mars Orbiter Laser Altimeter measurements has been presented by Soderblom and Kirk (2003). The images are registered onto a shaded depth map and the parameters of the reflectance model are then estimated until the estimated height matches the depth map in a least-squares sense. The resolution of the depth map increases by a factor of about 200 (Soderblom and Kirk, 2003). Both methods restrict variations of the reflectance parameters to the lateral resolution of the laser range scanning data, i.e. use area-wise constant parameters. This method has been applied to candidate landings sites for Mars Exploration Rovers by Kirk et al. (2003b). Furthermore, Kirk et al. (2003a) included this method into the ISIS software framework. By performing a fixed number of iterations, the photometric estimate yields an interpolation of an existing DEM

(Kirk et al., 2003a). This approach, however, does not constrain the solution of the photoclinometry towards the DEM. Although the lateral resolution of the DEM is captured by a smooth interpolation and mapping onto the image grid it is not further regarded during the optimisation. The least squares matching between the estimated surface and the a-priori DEM during the computation of the parameters of the reflectance model implicitly assumes that the mean depth of both DEMs is equal. Assuming that the resolution of the image is several times higher than the resolution of the a-priori DEM, the estimated surface will contain small scale features, e.g. craters and rocks, that are not contained in the a-priori DEM. These are likely to change the mean depth of the estimated surface. If these small scale features are not taken into account before the comparison it may influence the estimation of the photometric model.

Fassold et al. (2004) developed an algorithm for the fusion of a photometric depth estimation with a stereo DEM. However, their method is restricted to Lambertian reflectance and applies a smoothness regularisation. Unfortunately, planetary surfaces like that of the Moon do not show a Lambertian reflectance behaviour, and the smoothness regularisation tends to produce oversmoothed DEMs and, even worse, drives the obtained DEM away from the photometric optimum (Horn, 1990).

A method to combine depth from gradient fields and sparse depth data, e.g. known depth points, has been proposed by Horovitz and Kiryati (2004). The depth points are integrated into the optimisation using weighted least squares to limit the influence of single depth points. Horovitz and Kiryati (2004) present different weighting functionals. However, the choice of the weighting function affects the smoothness of the surface and thus limits the usability of the approach. A second method introduced by Horovitz and Kiryati (2004) is the correction of a previously estimated photometrically obtained DEM, which is achieved by interpolating the depth difference between the absolute depth data and the photometrically obtained DEM based on the thin plate equation. The thin plate equation yields a smooth interpolation behaviour and thus can be interpreted as the extraction of the low spatial frequency error which is inherent to photometric methods: Small errors of the gradient estimates accumulate during the integration step and tend to introduce a bias of the resulting surface at low spatial frequencies. The final DEM is then computed as the superposition of the photometrically obtained DEM and the interpolation function.

At the same time, Dorrer et al. (2004) proposed the de- and re-shading method for dense depth data of “sufficient quality”, regarding the example of the Mars Orbiter Wide Angle Camera. The existing DEM is added to the photometric optimisation problem as a soft constraint, i.e. a weighted error term describing the squared difference between the

optimised and the existing topography model is added to the overall error functional. The approach is restricted to Lambertian reflectance and uniform albedos. Similar to Soderblom and Kirk (2003), the different resolutions of the data sets are not taken into account. This approach has been demonstrated by Albertz et al., 2005, Kirk et al., 2006, considering data of the High Resolution Stereo Camera of the Mars Express spacecraft.

Another approach dealing with dense absolute depth data has been introduced by Nehab et al. (2005), who add the high spatial frequency components of the photometrically obtained DEM by rotating the smoothed surface normals estimated from the absolute depth data into the high-frequency component of the photometrically obtained surface normals.

Afterwards, the resulting gradient field is integrated by minimising the violation of an orthogonality constraint between the normals and the tangents of the estimated surface as well as minimising the Euclidean distance between the estimated DEM and the measured absolute depth data. The bias correction is applied in both cases after the estimation of the gradient field and is therefore not directly related to our work.

The method presented by Gaskell et al. (2008) uses a different way to constrain the photometric surface estimation. First, the average albedo and the background intensity are derived for each image. Then a mixture of the Lambert and the Lommel–Seeliger reflectance functions is applied to derive a relative albedo and the surface gradients at a randomly chosen pixel and its four nearest neighbours. The depth of the chosen pixel is then estimated by integrating the average gradient of the chosen and each of the four neighbouring pixels, respectively. The four results and a weighted constraining depth value are averaged to obtain the final depth value for the chosen pixel. This procedure is repeated until convergence is achieved (Gaskell et al., 2008).

Schenk (2002) has developed a method that independently computes stereo analysis and photoclinometry for the estimation of icy shells. The stereo DEM is used to control the long-wavelength component of the photoclinometry DEMs. This is achieved by merging the low-frequency component of the stereo DEM with the high-frequency component of the photoclinometry result. Later, Schenk (2008) applied these techniques to icy satellites and used the combination of stereo analysis and photoclinometry whenever possible.

The more recent method for the refinement of existing DEMs by Barron and Malik (2011) estimates the surface shape on small spatial scales simultaneously with the pixel-wise albedo based on a single image, assuming a Lambertian reflectance model. To separate the effects of the surface gradients and the albedo on the observed image intensities from each other, the statistical properties of “typical” albedo maps and surfaces are learned from examples. The approach allows for an integration of independently obtained depth

information obtained e.g. by stereo image analysis or active range scanning into the estimated small-scale surface data. The method is extended by Barron and Malik (2012) towards an additional estimation of the illumination conditions.

A different development is the inclusion of the photometric information into the stereo process. Lohse et al. (2006) optimise the surface in the object space. The surface is rendered using the photometric information and projected into the stereo cameras. The photometric error functional is then computed between the measured and the projected images. This method is most stable for oblique views. Since most spectral datasets are recorded using a nadir view, an additional sensor would be necessary. Additionally, Lohse et al. (2006) state that their method is sensitive to the reflectance model. Similarly, Gehrke (2006) includes photometric cues and the derivation of reflectance parameters into the facets stereo algorithm by Weisensee (1992). The algorithm, however, still requires oblique views.

The aforementioned methods include the absolute depth data in different ways, e.g. constraining the depth estimation, constraining the estimation of the reflectance model, fusing different datasets or initializing the method. To the best of the authors' knowledge, existing methods do not include absolute depth data into the photometric estimation of the gradient field. However, the gradient field is important for the normalisation of hyperspectral data since the surface slope is defined by the local gradient field on small spatial scales. Furthermore, no existing method deals with spatially varying non-Lambertian reflectance functions at image resolution, which is required for remote sensing of planetary bodies. These problems are addressed in this study. We present a method for the simultaneous estimation of locally varying parameters of an arbitrary but known reflectance model and the estimation of local gradients integrating photometrically obtained surface gradients and independently measured absolute depth data.

There are two distinct groups of models, namely empirical and analytical models. The empirical models, which are commonly used in photoclinometry and normalisation of spectral data, are reviewed by McEwen (1991). McEwen (1991) suggests a product of a functional depending on the phase angle and a Lommel–Seeliger law or a Minnaert function. The functional depending on the phase angle is set to be a wavelength dependent polynomial, as in the case of McEwen et al., 1998, Hicks et al., 2011.

The latter group consists on physically motivated, analytical functions. In case of the lunar surface the prominent models are Hapke, 2002, Shkuratov et al., 1999. Both models are based on the reflection of one particle which is modelled as a slab. The overall reflectance is then estimated by adding first or higher order scattering between multiple particles in a layer of regolith. The difference between Hapke, 1981, Shkuratov et al., 1999 is the

modelling of the single-particle scattering function which is also termed “phase function” (Poulet et al., 2002). While Shkuratov et al. (1999) predicts the functional, Hapke (1981) considers it a free parameter of the model. This also holds for Hapke (2002) which is an extension of higher order scattering to the original model. Additionally, Hapke (1984) proposed an extension to take into account the surface roughness unresolved by the detector. The proposed extension is valid for arbitrary reflectance models.

According to Bertsatos and Makris (2010), small-scale albedo changes dominate the photometric error and thus a simultaneous estimation of the reflectance parameters is necessary. Due to the typically large number of parameters, empirical modelling is not suitable for a simultaneous surface reconstruction and reflectance parameter estimation. Although it is possible to limit the parameters of the empirical models, e.g. by decreasing the order of the polynomial, the accuracy of the model decreases. Furthermore, the estimated parameters of the phase function are often global or semi-global estimates, such as in McEwen et al., 1998, Hicks et al., 2011, which contradicts the necessity for parameter estimation on small spatial scales. Furthermore, McEwen (1991) states that the Hapke model provides accurate fits to planetary surfaces and relates all regarded photometric functions to the model by Hapke, 1981, Hapke, 1984, Hapke, 1986. The reason for using the Minnaert and Lommel–Seeliger laws is given by their low computational complexity. Efford (1991) shows that the empirical models do not cover the effect of macroscopic roughness and thus lead to biased topography profiles. In principle it is possible to apply the extension proposed by Hapke (1984) to the empirical models but the computational complexity is greatly increased. Hence, we will focus on the Hapke model itself.

The proposed algorithm requires co-registered photometric data and depth data of lower lateral resolution. In order to avoid a remapping and registration of different coordinate systems, we select data sets that are already mapped to the coordinate system of the Lunar Reconnaissance Orbiter (LRO).

A recently released hyperspectral data set of the Moon has been obtained by the Moon Mineralogy Mapper (M^3) instrument¹ carried by the Indian spacecraft Chandrayaan-1. According to Pieters et al. (2009), the M^3 sensor is a pushbroom camera which scans lines with a ground pixel size of about 140m. In the so called “global mode”, it provides 85 channels measuring the spectral radiance in the range between 450 and 3000nm. The filter width of each channel is about 10nm. There is also a so-called “target mode” of higher spectral resolution. However, its coverage is limited to a few regions of interest. Thus, we restrict our study to global mode measurements. Although it is possible to use several spectral channels in our DEM construction framework, we base our surface reconstructions on the channel centred at 1579nm which, in our experience, shows a high signal-to-noise

ratio and does not fall in a possible spectral absorption feature. Since we aim for a normalisation routine of the spectral data, the reflectance parameter estimation routines are applied to all channels, producing spectra of parameters. The further normalisation steps and an interpretation of the spectral data, however, are beyond the scope of this paper. The M^3 radiance data are accompanied by the spectral solar irradiance, the coordinates of each pixel in selenographic longitude and latitude, and, pixelwise, the solar distance, the solar zenith and azimuth angles with respect to a spherical body, as well as the direction toward the spacecraft. These angles and derived vectors allow the computation of all necessary angles with respect to an arbitrary surface normal.

The M^3 images are published as measured by the pushbroom sensor, i.e. as a concatenation of scanlines. The spatial distance between two subsequent scanlines is not constant. Furthermore, our DEM construction method is based on a cylindrical projection of the spherical body which spans a rectangular grid, i.e. the selenographic longitude is the first unit vector and the selenographic latitude is the second unit vector. We resample the data to the selenographic coordinate system using a fixed grid with 300 pixels per degree latitude and longitude, respectively. This corresponds to about 100m per pixel and avoids subsampling effects. Interpolation is performed using the natural neighbour method (Sibson, 1981). Fig. 2(a) shows a resampled M^3 image of the crater Aristarchus (longitude **312°E–314°E**, latitude **22°N–26°N**).

Fig. 3(a) shows a global mosaic of the reflectance averaged over all M^3 images at 1579nm at a resolution of 2 pixels per degree longitude and latitude. It extends to a latitude of $\pm 60^\circ$. The brightness variations are due to different illumination conditions and missing spectral normalisation. The corresponding number of co-registered images from different orbits is shown in Fig. 3(b). Fig. 3(c) and (d) show the minimum and maximum incidence angles. Due to the nadir orientation of the instrument, the emission angles are always close to zero. The maximum interval of the incidence angle for a specific region is about 60° while it is usually below 40° . This small interval of incidence and thus also phase angles does not allow for an estimation of all surface parameters, since phase angles larger than 90° are completely missing. According to Bertsatos and Makris (2010), the phase function is approximately constant over a small range of phase angles and the albedo variations dominate the error of photoclinometry. Thus, we limit our estimation of surface parameters to the single-scattering albedo, and we include the asymmetry parameter of the phase function if the range of available phase angles exceeds 20° (cf. Section 4).

Two global topographic datasets have recently been published, namely the Lunar Orbiter Laser Altimeter (LOLA) DEM² (Smith et al., 2010, Zuber et al., 2010) and the “near-global lunar 100m raster DEM”³ (GLD100) (Scholten et al., 2012).

The Lunar Orbiter Laser Altimeter (LOLA) carried by the Lunar Reconnaissance Orbiter (LRO) spacecraft provides time-of-flight range measurements. Based on ground truth measurements, the standard deviation of the one-way laser ranging is 0.1 m (Riris et al., 2009). This precision is significantly higher than the capability to track the spacecraft's orbit (Zuber et al., 2010). According to Zuber et al. (2010), the precision of ± 0.1 m is achieved only for the polar topography measurements while the global depth error is higher than ± 1 m at a lateral resolution of 50 m along the measured track. A gridded global DEM has been derived by binning the point measurements and interpolating empty bins, which shows interpolation artifacts between different tracks (Neumann, 2010). In this study, we use for the surface reconstruction the global DEM published at a lateral resolution of 512 pixels per degree, which corresponds to about 60 m per pixel near the lunar equator. The regions of interest are cropped from the original map and resized to the 300 pixels per degree resolution of our resampled M^3 data. The shaded LOLA DEM of the crater Aristarchus is shown in Fig. 2(b) and clearly reveals interpolation artifacts. Hence, the effective lateral resolution is lower than the 100 m of the grid. Due to the very high accuracy, we use the single-point measurements as ground truth and compare the reconstructed DEMs to these.

The GLD100 is a nearly global DEM obtained by stereo analysis of images taken by the Wide Angle Camera (WAC) carried by LRO. The nominal resolution of the GLD100 is 100 m per pixel (Scholten et al., 2012). We resample the GLD100 data to our M^3 grid. Fig. 2(c) shows the shaded GLD100 for the crater Aristarchus. Due to the area-based correspondence matching approach inherent to the employed stereo analysis method, small-scale features with an extent of less than 1.5 km are likely to be not or inaccurately represented within the GLD100 data (Scholten et al., 2012), such that the effective lateral resolution of the GLD100 is significantly lower than the resolution of the M^3 hyperspectral data.

In summary, both available global lunar DEMs do not share the lateral resolution of the M^3 hyperspectral data. Therefore, our method aims to increase the lateral DEM resolution to the resolution of the M^3 data. The result for the crater Aristarchus is presented in Fig. 2(d).

Access through your organization

Check access to the full text by signing in through your organization.

Access through **your organization**

Section snippets

Outline

The proposed algorithm consists of several steps. An overview is given in Fig. 4. To ensure co-registered depth and image data, an illumination-independent image registration scheme is applied. This step is optional and may be omitted if the datasets are already aligned. Afterwards, the parameters of the reflectance model are estimated pixel-wise and an extended PHCL scheme is applied to estimate the surface gradients. The proposed PHCL scheme constrains the surface gradient estimates using the ...

Theoretical background

The DEM construction method proposed in this work is rooted in the variational shape from shading algorithm by Horn (1990). For the sake of completeness, this section introduces the important physical quantities, reviews the original algorithm and presents an extension towards image grids with non-uniform ground pixel sizes. ...

Reflectance modelling of the lunar surface

The so-called “reflectance function” R of a surface (sometimes also termed “photometric function”) is given by the ratio between the observed surface radiance L and the irradiance E . In general, the amount of light reflected from the surface depends on the surface normal \mathbf{n} , the direction \mathbf{s} to the light source, the direction \mathbf{v} to the camera, and inherent surface properties (Horn et al., 1986). For planetary surfaces, where the intensity of the light reflected from the surface is independent of ...

Construction of DEMs of high lateral resolution

We construct DEMs of a lateral resolution corresponding to that of the available images by fusion of high-resolution image data and DEMs of lower lateral resolution. This section describes two independent methods. The first approach is based on the estimation of surface gradients and a subsequent recovery of the surface from the estimated gradient field. The second approach extends the shape from shading scheme proposed by Horn (1990) to include the existing DEM data by imposing large-scale ...

Results and discussion

The evaluation of the proposed methods is not straightforward since there are no “ground truth” data available for direct comparison. Hence, the proposed reconstruction methods are first evaluated based on synthetic “ground truth” data, and then based on single LOLA measurements that have a vertical accuracy of about 1 m but do not cover the full examined areas. Finally, the image registration is evaluated using the proposed method to transform the images into a 3D space and compute the ...

Summary and conclusion

In this study we have introduced an image-based framework for the construction of lunar DEMs of high lateral resolution. Existing lunar DEMs obtained based on laser altimetry (LOLA DEM) or photogrammetric measurements (GLD100) are accurate on large spatial scales while displaying noise on small spatial scales. In contrast, intensity-based surface reconstruction methods such as photometric stereo and shape from shading reveal small-scale surface details but tend to become inaccurate on large ...

[Special issue articles](#) [Recommended articles](#)

References (80)

I. Bertatos *et al.*

[Statistical biases and errors inherent in photoclinometric surface slope estimation with natural light](#)

Icarus (2010)

A. Dollfus

[Lunar Surface Imaging Polarimetry. I: Roughness and grain size](#)

Icarus (1998)

B. Hapke

[Bidirectional reflectance spectroscopy. 3: Correction for macroscopic roughness](#)

Icarus (1984)

B. Hapke

[Bidirectional reflectance spectroscopy. 4: The extinction coefficient and the opposition effect](#)

Icarus (1986)

B. Hapke

[Bidirectional Reflectance Spectroscopy. 5: The coherent backscatter opposition effect and anisotropic scattering](#)

Icarus (2002)

B.K.P. Horn

[Understanding image intensities](#)

Artificial Intelligence (1977)

I. Horowitz *et al.*

[Depth from gradient fields and control points: bias correction in photometric stereo](#)

Image and Vision Computing (2004)

V. Lohse *et al.*

[Derivation of planetary topography using multi-image shape-from-shading](#)

Planetary and Space Science (2006)

A.S. McEwen

[Photometric functions for photoclinometry and other applications](#)

Icarus (1991)

A.F. McGuire *et al.*

[An experimental study of light scattering by large, irregular particles](#)

Icarus (1995)



[View more references](#)

Cited by (65)

[Centimeter-resolution topographic modeling and fine-scale analysis of craters and rocks at the Chang'E-4 landing site](#)

2021, Earth and Planetary Science Letters

[Show abstract](#) ✓

[An integrated photogrammetric and photoclinometric approach for illumination-invariant pixel-resolution 3D mapping of the lunar surface](#)

2020, ISPRS Journal of Photogrammetry and Remote Sensing

[Show abstract](#) ✓

Construction of pixel-level resolution DEMs from monocular images by shape and albedo from shading constrained with low-resolution DEM

2018, ISPRS Journal of Photogrammetry and Remote Sensing

Citation Excerpt :

...The incorporation of existing low-resolution DEMs into SAfS algorithms using single or multiple images combines the geometric accuracy of low-resolution DEMs and the pixel-level reconstruction ability of SAfS. Algorithms have been explored and developed (Barron and Malik, 2012; Grumpe et al., 2014) with promising results. A low-resolution DEM provides a constraint over shape geometry and encourages the resulting DEM from SAfS to comply with the general geometry of the low-resolution DEM....

[Show abstract](#) ✓

Integrated topographic, photometric and spectral analysis of the lunar surface: Application to impact melt flows and ponds

2014, Icarus

[Show abstract](#) ✓

Multiview Shape-From-Shading for Planetary Images ↗

2018, Earth and Space Science

Time-of-day-dependent global distribution of lunar surficial water/hydroxyl ↗

2017, Science Advances



[View all citing articles on Scopus](#) ↗

[View full text](#)

Copyright © 2013 COSPAR. Published by Elsevier Ltd. All rights reserved.



All content on this site: Copyright © 2025 Elsevier B.V., its licensors, and contributors. All rights are reserved, including those for text and data mining, AI training, and similar technologies. For all open access content, the relevant licensing terms apply.

